High-rate reactive ion etching of barium hexaferrite films using optimal CHF_3/SF_6 gas mixtures

Zhaohui Chen,[1,a)] Aria Yang,[1] Changqing Xie,[2] Qinghua Yang,[2] C. Vittoria,[1] and V. G. Harris[1]

[1]*Center for Microwave Magnetic Materials and Integrated Circuits and Department of Electrical and Computer Engineering, Northeastern University, Boston, Massachusetts 02115 USA*
[2]*Key Laboratory of Nano-Fabrication and Novel Devices Integrated Technology, Institute of Microelectronics, Chinese Academy of Sciences, Beijing 100029 People's Republic of China*

(Received 29 December 2008; accepted 24 February 2009; published online 18 March 2009)

The high-rate reactive ion etching of *c*-axis oriented quasi-single-crystal barium hexaferrite (Ba*M*) films, deposited on 6-*H* silicon carbide (0001) substrates, has been demonstrated. Arrays of Ba*M* columns, having diameters of 1–4 μm and sharp vertical walls, were etched from Ba*M* films at rates as high as 75 nm/min using an optimized sulfur hexafluoride and methyl trifluoride (SF_6:CHF_3, 3:1) gas mixture. Lateral features as small as 43 nm were fabricated and imaged.
© *2009 American Institute of Physics*. [DOI: 10.1063/1.3099884]

It has been a long-standing goal of the microwave electronics community to integrate microwave passive devices (e.g., circulators, isolators, phase shifters, filters, etc.) with semiconductor device platforms. Such an achievement would meet the demands of increasing systems integration, while concomitantly reducing device profile, volume, and weight.[1] Realizing practical integration relies upon two key technological advances: (i) the growth of oriented, high crystal quality magnetic oxide films on semiconductor substrates and (ii) the patterning of magnetic oxide films into device and integrated circuit structures. The processing of semiconductor film structures, including film deposition and patterning, has been well established, while similar processing of magnetic oxide film structures on semiconductor substrates remains a significant challenge. Previously, we have demonstrated the growth by pulsed laser deposition of *c*-axis oriented, quasi-single-crystal, barium hexaferrite (Ba*M*) (i.e., $BaFe_{12}O_{19}$) films on wide-band-gap semiconductor substrates, SiC[2–4] and GaN.[5] Using such films as seed layers for growth by liquid phase epitaxy,[6–9] films of more than 100 μm can be realized. This approach provides a reasonable pathway to integrating ferrite films, having the necessary thickness and crystal quality for microwave devices, with semiconductor platforms. Alternatively, the patterning of near- and submicron features in Ba*M* and other ferrites has received considerably less attention and remains a significant challenge in realizing practical oxide-based microwave electronics. It is widely acknowledged that the depth control afforded by wet etching of ferrites is a key limitation.[10] Attempts at dry etching ferrite materials, using Ar ions and laser thermal etching,[11–13] resulted in severe lateral overetching and excessive film damage. In addition, no isotropic etching processes can reliably provide submicron lateral features.

The Ba*M* films used in this study had thicknesses ranging from 0.5 to 2.0 μm and were grown by pulsed laser deposition (PLD) on single crystal 6-*H* SiC substrates. The details of the film growth are presented elsewhere.[2–4] Due to the alignment of the crystallographic *c*-axis perpendicular to the film plane together with low microwave loss, such films are uniquely suited for many microwave device applications. However, the demagnetization energy inherent in thin films acts to align the spontaneous magnetization vector along the film plane, thus requiring large bias magnets to polarize and saturate the ferrite film for device operation. Bias magnets used in conventional passive devices are often heavy and voluminous constructs that limit attempts at planar integration. In realizing self-biased microwave passive devices, we propose the patterning of Ba*M* films into arrays of cylindrical pillars. The demagnetizing field of the columns is expected to reduce the demagnetizing energy of the film and assists in the realignment of the spontaneous magnetization along the long axis of the columns. Additionally, a pillar array may also be used as a seed layer in the growth of thicker films by liquid phase epitaxy having unique and favorable microstructure. In this letter, the high-rate reactive ion etching of *c*-axis oriented quasi-single-crystal barium hexaferrite films, deposited on SiC substrates, is reported. Ba*M* columns, having diameters of 1–4 μm and sharp vertical walls, were etched from Ba*M* films at rates as high as 75 nm/min using SF_6 and CHF_3 gas mixtures. High resolution etching of lateral features as small as 43 nm were realized.

The etching experiments were performed using an ICP-98A system at the Institute of Microelectronics, Chinese Academy of Sciences. Before etching, optical lithography was performed to transfer the photomask test pattern to the photoresist (Shipley AZ5214-E). The depths of the pillars were measured after the dry etching process using a Veeco DekTak surface profilometer. The estimated error in the depth profile was ~20 nm, which was considered in the estimated etch rate uncertainty.

In the reactive ion etch (RIE) process, the following three important parameters were optimized: (i) the process gas mixture, (ii) the chamber pressure, and the (iii) capacitive electrode rf power. During the film etching, the plasma chamber was evacuated to a dynamic vacuum of $\sim 10^{-6}$ Torr, maintained by a gas flow of 240 standard cubic centimeter per minute in concert with the conductance of the

a)Author to whom correspondence should be addressed. Tel.: +1 617-373-5160. Electronic mail: zchen@ece.neu.edu.

 © 2009 American Institute of Physics

Downloaded 20 Mar 2009 to 129.10.56.212. Redistribution subject to AIP license or copyright; see http://apl.aip.org/apl/copyright.jsp

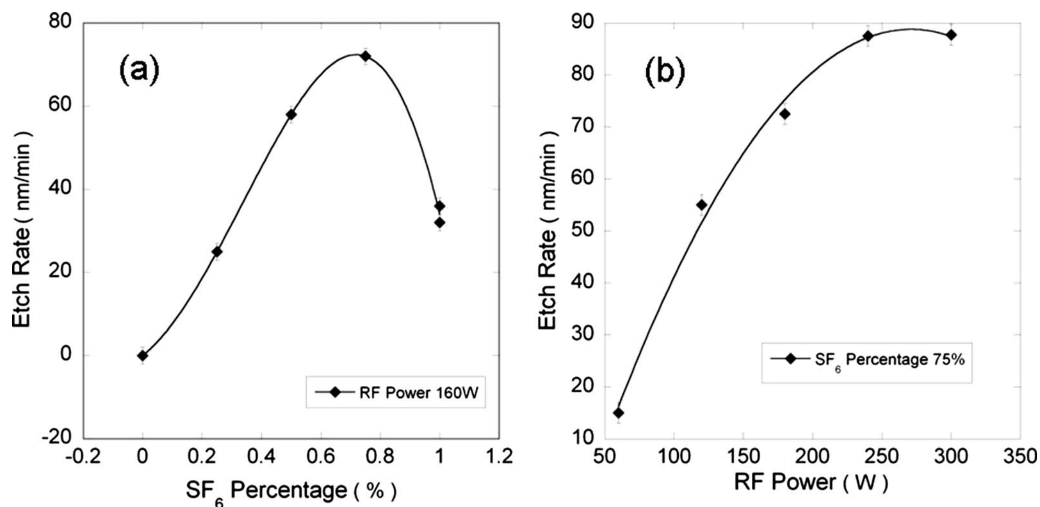

FIG. 1. The etch rates of Ba*M* films as a function of gas mixtures (a) and rf power (b). The data in panel (a) were collected using an rf power of 160 W.

turbomolecular pump. The sample holder was water cooled to maintain a fixed sample temperature of ~27 °C to minimize thermally induced damage to the film sample. An initial gas mixture of CHF_3/Ar (5:2), similar to that used in conventional SiO_2 etching, as well as CHF_3 alone, resulted in only slight etching of the sample and little removal of film mass. The Ba*M* film was only effectively etched after the CHF_3 was mixed with SF_6. The optimal ratio of $CHF_3:SF_6$, 1:3 was achieved through the systematic variation of gas mixtures and repeated evaluation of the etched patterns. The dependency of the etch rate to gas mixture is illustrated in Fig. 1(a). During measurements, the electrode rf power was maintained at 160 W. These results indicate that the presence of SF_6 was critical and acted as the primary reactive gas. We postulate that the SF_6 gas produced most of the ions and erosive neutrals, which were dissociated in the plasma environment to form atomic fluorine. Atomic fluorine in turn reacted with the Ba*M* film to form volatile BaF_x and FeF_x gas complexes that were exhausted by the vacuum system. However, when only SF_6 gas was employed, the etch rate remained lower than that of the $CHF_3:SF_6$ gas mixtures. This indicates that the CHF_3 was not only a buffer gas that maintained plasma stability but also provided additional energetic ions that enhanced the ionization of the SF_6 molecules.

In a second study, using an optimized 1:3 CHF_3/SF_6 mixture, the electrode rf power was varied to study its impact upon the etching profile. For each trial, etching was performed for a total of 5 min., as a function of electrode rf power. The etch rate was determined and plotted in Fig. 1(b). From these data, the etching threshold power was determined to be ~60 W, with a maximum etching rate of ~87 nm/min, corresponding to ~240 W of rf power. However, the application rf power greater than ~200 W resulted in the over etching of patterned sidewalls. The maximum rf power that resulted in high etch rates and high quality etched structures was ~160 W.

Figures 2(a)–2(c) are scanning electron microscopy (SEM) images of the top view (a), side view (b), and ex-

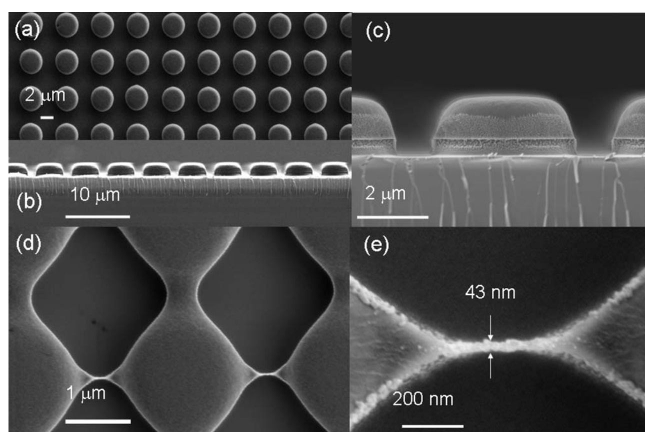

FIG. 2. Top-view SEM image of the patterned Ba*M* film array consisting of ~3 μm diameter pillars at a ~4 μm center-to-center spacing (a). Film was etched using an optimal gas mixture and rf power. Side-view SEM image of the same sample (b). An expanded view of one pillar consisting of a Ba*M* cylinder with height to diameter aspect ratio of 0.2 having a photoresist cap on the surface (c). The "frost" on the element is a thin PtPd coating used to reduce fluorescence during SEM imaging. Top view SEM image of a test pattern designed to evaluate minimum lateral features (d). An expanded view of the minimal lateral feature of ~43 nm (at the necked region) (e).

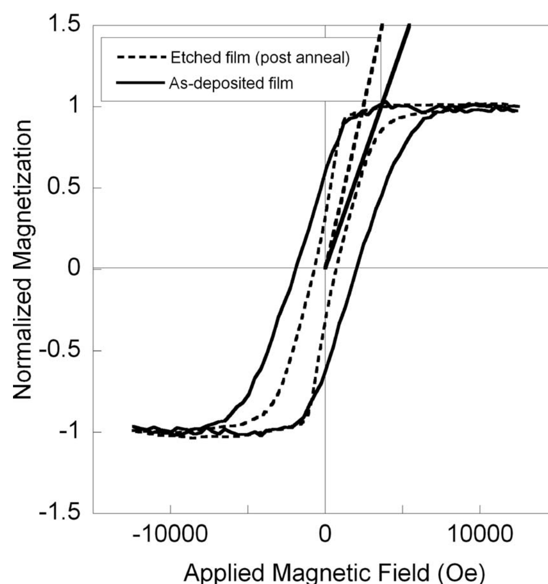

FIG. 3. Hysteresis loops, as normalized magnetization vs applied magnetic field in Oe, for the as-deposited film sample (solid line) and etched film after annealing (dashed line). The lines correspond to the slope of the loops as they pass through remanence and qualitatively reflect the sample's demagnetizing energies.

Downloaded 20 Mar 2009 to 129.10.56.212. Redistribution subject to AIP license or copyright; see http://apl.aip.org/apl/copyright.jsp

TABLE I. Demagnetizing fields (H_d), coercive fields (H_c), and demagnetizing factors (N) of as-deposited Ba*M* film, after etching, and after etching followed by a heat treatment. Note: %Δ represents percent change from as-deposited condition. N_t was approximated using the oblate ellipsoid model, $N_t = m^2/(m^2-1)\{1-[1/(m^2-1)^{1/2}]\arcsin[(m^2-1)^{1/2}/m]\}$, where m represents aspect ratio of pillar.

	H_d(%Δ) (Oe)	H_c^e(%Δ) (Oe)	H_c^h(%Δ) (Oe)	N_t(%Δ)	N_e(%Δ)
As-deposited film	3886	1600	189	0.99	0.97
Etched film	3137 (−19.3%)	2000 (+25%)	332 (+75.7%)	0.75 (−24.2%)	0.78 (−19.6%)
Etched film after anneal	3100 (−20.3%)	756 (−52.8%)	39 (−79.4%)	0.75 (−24.2%)	0.77 (−20.6%)

panded side view (c) of the optimized etched pillar array and individual elements. The images reveal a clear array of periodic cylindrical elements. The expanded view depicted in Fig. 2(c) reveals each element in the array to consist of a cylinder of Ba*M* capped with photoresist. The aspect ratios of column height to diameter for all samples of the present study ranged from 0.2 to 1.0. Figures 2(d) and 2(e) are top view SEM images of a Ba*M* test pattern revealing a minimum lateral feature of 43 nm [Fig. 2(e)]. Control of patterned features on such a scale proves the viability of this etching procedure as a means to fabricate future nanoscale magnetic oxide integrated circuits.

An important consideration of the etching procedure is its impact upon the film's magnetic properties. Since damage to the Ba*M* film is anticipated, it is unclear if the films will be suitable for magnetoelectronics applications after etching. Properties are ascertained for the as-deposited film, after etching, and after a heat treatment at 1050 °C in air for a period of 25 min. In Fig. 3, the hysteresis loops, as normalized magnetization versus applied field, for the as-deposited film and the etched film after annealing, are presented. The loops clearly illustrate improved losses as well as a reduced demagnetizing field in the etched film. These results are made clear in Table I, where we present the demagnetizing field (H_d), the coercive fields [collected with the applied field aligned along both the easy, (H_c^e) and hard (H_c^h) directions], and the theoretical and experimental demagnetizing factors N_t and N_e, respectively. As discussed earlier, one goal of etching pillar arrays in the Ba*M* films was to reduce the demagnetizing field in hopes of establishing a self-biased magnetized state. Alternatively, the coercive fields are important parameters in that they are acutely sensitive to defects and structural imperfections and reflect the static magnetic losses in the film/pillar arrays. As seen in Table I, etching the pillar array significantly reduced the demagnetizing field of the as-deposited film; a reduction of 19.3%. As anticipated, the etching procedures raised the coercivity (25%) from the as-deposited state. However, postetching heat treatment proved effective in healing etching induced defects, resulting in a 52.8% decrease in H_c^e. These improvements were mirrored in values of H_c^h (reduction of 79.4%). Examining the demagnetizing factor, one sees that the theoretical values are well matched by experiment. These findings confirm that the demonstrated etching process was effective in not only patterning magnetic oxides films but also in maintaining desirable magnetic properties of the patterned structures necessary for development of microwave integrated circuits.

In summary, the mixture of SF_6 and CHF_3 was found effective in the reactive ion etching of *M*-type barium hexaferrite. The presence of CHF_3 was shown to be important to both the etching rate and the quality of vertical sidewall profiles. The optimum gas mixture was a ratio of one part CHF_3 to three parts SF_6, with an electrode rf power of 160 W. These conditions lead to the maximum effective etch rate of ~75 nm/min and the patterning of nanoscale features of less than 50 nm in films as thick as 2 μm. The magnetic properties, especially those reflecting magnetic loss, were shown to degrade with etching. However, postetching heat treatments showed that the magnetic properties were recovered and even improved relative to their virgin state. The high rate etching of magnetic oxides, and specifically microwave ferrites as demonstrated here, is an essential advancement that enables fabrication of planar microwave devices and their ultimate integration with semiconductor integrated circuit platforms.

This work was supported, in part, by the Office of Naval Research (Grant No. N00014-05-10349) and the National Science Foundation (Grant No. DMR 0400676). The authors thank Chen Lu, Jihong Tian, Yajie Chen, and William H. Fowle for their technical assistance and helpful discussions.

[1] V. G. Harris, Z. Chen, Y. Chen, S. D. Yoon, T. Sakai, A. Geiler, A. Yang, Y. He, K. S. Ziemer, N. Sun, and C. Vittoria, J. Appl. Phys. **99** 08M911 (2006).
[2] Z. Chen, A. Yang, S. D. Yoon, K. Ziemer, C. Vittoria, and V. G. Harris, J. Magn. Magn. Mater. **301**, 166 (2006).
[3] Z. Chen, A. Yang, Z. Cai, K. Ziemer, C. Vittoria, and V. G. Harris, IEEE Trans. Magn. **42**, 2855 (2006).
[4] Z. Chen, A. Yang, A. Geiler, V. G. Harris, C. Vittoria, P. R. Ohodnicki, K. Y. Goh, M. E. McHenry, Z. Cai, T. L. Goodrich, and K. S. Ziemer, Appl. Phys. Lett. **91**, 182505 (2007).
[5] P. R. Ohodnicki, K. Y. Goh, Y. Hanlumyuang, K. Ramos, M. E. McHenry, Z. Cai, K. Ziemer, H. Morkoc, N. Biyikli, Z. Chen, C. Vittoria, and V. G. Harris, J. Appl. Phys. **101**, 09M521 (2007).
[6] S. G. Wang, S. D. Yoon, and C. Vittoria, J. Appl. Phys. **92**, 6728 (2002).
[7] S. D. Yoon and C. Vittoria, J. Appl. Phys. **93**, 8597 (2003).
[8] M. S. Yuan, H. L. Glass, and L. R. Adkins, Appl. Phys. Lett. **53**, 340 (1988).
[9] Y. Song, J. Das, Z. Wang, W. Tong, and C. E. Patton, Appl. Phys. Lett. **93**, 172503 (2008).
[10] U.S. Patent No. 4,875,970 (29 October 1989).
[11] E. K. Yung, B. W. Hussey, A. Gupta, and L. T. Romankiw, J. Electrochem. Soc. **136**, 665 (1989).
[12] Y. F. Lu, M. Takai, S. Nagamoto, and S. Namba, Appl. Phys. B: Lasers Opt. **53**, 39 (1991).
[13] M Takai, S Nagatomo, H Kohda, C Yada, H Sandaiji, Appl. Phys. A: Solids Surf. **58**, 359 (1994).

Downloaded 20 Mar 2009 to 129.10.56.212. Redistribution subject to AIP license or copyright; see http://apl.aip.org/apl/copyright.jsp